Photodissociation dynamics of the HCNN radical

Ann Elise Faulhaber, Jason R. Gascooke,[a] Alexandra A. Hoops,[b] and Daniel M. Neumark[c]
Department of Chemistry, University of California, Berkeley, California 94720 and Chemical Sciences Division, Lawrence Berkeley National Laboratories, Berkeley, California 94720

(Received 18 January 2006; accepted 24 March 2006; published online 22 May 2006)

The photodissociation dynamics of the diazomethyl (HCNN) radical have been studied using fast radical beam photofragment translational spectroscopy. A photofragment yield spectrum was obtained for the range of 25 510–40 820 cm^{-1}, and photodissociation was shown to occur for energies above 25 600 cm^{-1}. The only product channel observed was the formation of CH and N_2. Fragment translational energy and angular distributions were obtained at several energies in the range covered by the photofragment yield spectrum. The fragment translational energy distributions showed at least two distinct features at energies up to 4.59 eV, and were not well fit by phase space theory at any of the excitation energies studied. A revised C–N bond dissociation energy and heat of formation for HCNN, $D_0(HC-NN)=1.139\pm0.019$ eV and $\Delta_f H_0(HCNN)=5.010\pm0.023$ eV, were determined. © *2006 American Institute of Physics*. [DOI: 10.1063/1.2196890]

I. INTRODUCTION

This paper reports the first investigation of the ultraviolet spectroscopy and photodissociation dynamics of the diazomethyl (HCNN) radical. HCNN and other HCN_2 isomers are of interest because of the possible role of the reaction of CH with N_2 in the formation of "prompt" NO in the combustion of hydrocarbon fuels.[1] Prompt NO formation is one of two NO formation mechanisms known to be important in the combustion of clean hydrocarbon fuels; the other is the well-understood thermal NO mechanism, which involves the attack of O atoms on N_2. Prompt NO formation occurs in the primary reaction zone of a hydrocarbon flame, where thermal NO formation is not possible because temperatures are too low for adequate concentrations of O atoms to be generated, and the observed rates of NO formation can only be explained by a lower-energy mechanism for the splitting of the N_2 bond. There is still a great deal of uncertainty about the reactions involved in prompt NO formation.

Prompt NO formation was discovered by Fenimore.[2] The reaction of CH with N_2 was one possibility proposed by Fenimore for the first step in producing prompt NO. In particular, he suggested the spin-forbidden reaction:

$$CH(X\,^2\Pi) + N_2(X\,^1\Sigma_g^+) \rightarrow HCN(\tilde{X}\,^1\Sigma) + N(^4S), \qquad (1)$$

followed by oxidation of N and HCN to form NO.

Fenimore's proposal has motivated many experimental[3–8] and theoretical[3,9–21] studies of the reaction of CH and other carbon and hydrocarbon radicals with N_2. Blauwens *et al.*[22] determined the concentration profiles of all the carbon and hydrocarbon fragments likely to be involved in prompt NO formation in the combustion of ethylene, ethane, and methane, and found only CH and CH_2 to correlate with NO. Furthermore, estimates of the rate constants for reactions of CH_2 with N_2 which could potentially lead to NO formation indicate that they are probably too slow to make a significant contribution.[1] Together, these findings provided some evidence that the $CH+N_2$ reaction is at least partially responsible for prompt NO formation. Various theoretical studies[10,12,16,18] have identified a cyclic C_{2v} isomer of HCN_2 (*c*-HCNN) as an intermediate in reaction (1), and have not shown HCNN to be along the reaction pathway (in fact, there is a barrier of about 2.38 eV between HCNN and *c*-HCNN according to Cui and Morokuma[16]). However, some calculations of the rate constant for reaction (1) (Refs. 17 and 21) indicate that it is far slower than the experimentally observed rate of CH removal,[4,5] suggesting that another mechanism may be operating in prompt NO formation.

More recently, Moskaleva and co-workers[13,15] proposed that the spin-allowed, endothermic reaction,

$$CH(X\,^2\Pi) + N_2(X\,^1\Sigma_g^+) \rightarrow NCN(\tilde{X}\,^3\Sigma_g^-) + H(^2S), \qquad (2)$$

is considerably faster than reaction (1) and may in fact be the first step in prompt NO formation. These results were supported in more recent calculations by Takayanagi.[23] In the proposed mechanism for reaction (2), *c*-HCNN formed from reactants and isomerizes to HNCN, which then falls apart to form H and NCN. A recent experimental study by Bise *et al.*[24] on the photodissociation dynamics of the HNCN free radical showed that it dissociates on the ground state surface to form CH and N_2, and suggested that a cyclic intermediate is involved. This provided evidence for a low-energy pathway between the reactants, CH and N_2, and HNCN consistent with the proposed mechanism for reaction (2).

In this work, we continue our investigation of the global $CH+N_2$ potential energy surface by studying the photodissociation dynamics of HCNN. There have been relatively

[a]Present address: Department of Chemistry, University of Adelaide, South Australia 5005, Australia.
[b]Present address: Combustion Research Facility, Sandia National Laboratories, Livermore, CA 94551.
[c]Author to whom correspondence should be addressed. Electronic mail: dneumark@berkeley.edu

few experimental studies of HCNN. Bise *et al.*[25] determined the heat of formation, $\Delta_f H_0(\mathrm{HCNN}) = 5.02 \pm 0.18$ eV, based on their experimentally determined value of $\Delta_f H_0(\mathrm{CNN})$ and the value of $D_0(\mathrm{H-CNN})$ for H atom loss previously determined by Clifford *et al.*[26] Infrared spectra of HCNN and DCNN were measured in inert gas matrices following the photolysis of H_2CNN and $(H/D)_2CNN$ with a mercury lamp, but the absorptions were not assigned.[27] Decay of the HCNN signal, attributed to photodissociation, was observed after longer irradiation with a mercury lamp; it was determined that photon energies below 16 000 cm^{-1} did not contribute to HCNN loss.[28] Photoelectron spectra of $HCNN^-$ and $DCNN^-$ were taken at 3.531 eV,[26] and the electron affinity of HCNN was determined to be 1.684 ± 0.006 eV. Vibrational spacings were seen at 485 ± 70 and 1780 ± 77 cm^{-1}, and were assigned as υ_5, the in-plane N–N–CH bend, and υ_2, the asymmetric N–N–CH stretch of HCNN, respectively, on the basis of frequencies obtained from *ab initio* calculations (537 cm^{-1} for υ_5 and 1879 cm^{-1} for υ_2). In the same study, the $\tilde{A}\,^2A'$ state of the neutral was determined to lie between 0.522 and 0.675 eV above the $\tilde{X}\,^2A''$ ground state. The equilibrium geometry of the ion was found to be very similar to that of HCNN ($\tilde{X}\,^2A''$), but quite different from that of HCNN ($\tilde{A}\,^2A'$). A study of the relaxation of CH ($X\,^2\Pi$, $\upsilon = 1$) by N_2 found a rapid relaxation rate, indicating the formation of a strongly bound complex, which the authors identified as HCNN.[29]

The $\tilde{X}\,^2A''$ state of HCNN has been treated by various electronic structure calculations,[10–12,16,18,21,26,30,31] and the $\tilde{A}\,^2A'$ state by a subset of these.[16,26,30] Both of these states correlate adiabatically to CH ($X\,^2\Pi$)+N_2 ($X\,^1\Sigma_g^+$). Cui and Morokuma[16] found the $\tilde{A}\,^2A'$ state to lie 0.48 eV above the ground state, in reasonable agreement with the experimental range reported by Clifford *et al.*[26] The same study placed HCNN $\tilde{X}\,^2A''$ 1.21 eV below CH ($X\,^2\Pi$)+N_2 ($X\,^1\Sigma_g^+$). The $\tilde{X}\,^2A''$ state is a datively bonded structure with C_s symmetry. The main difference between the geometries of the $\tilde{X}\,^2A''$ and $\tilde{A}\,^2A'$ states is the H–C–N bond angle, which is about 116° in the $\tilde{X}\,^2A''$ state, but about 150°, and very sensitive to the level of theory used, in the $\tilde{A}\,^2A'$ state.

There has been very little work on higher lying electronic states of HCNN. Using high level *ab initio* calculations, Cui and Morokuma[16] found the lowest lying quartet state, HCNN($a\,^4A''$), to lie 2.05 eV above the ground state. Another *ab initio* study found vertical transition energies of 1.86, 4.81, and 4.95 eV from the ground state.[30] The author suggested that the upper states were Rydberg levels but made no further comment on their nature or electronic configuration.

In this work we present the results of photodissociation dynamics studies of HCNN at energies of 3.351–4.454 eV. There are many product channels open for the dissociation of HCNN at these excitation energies. Several channels lead to the formation of CH and N_2, and are listed along with ΔH_0 for each reaction. ΔH_0 for channel (3) was determined in this study; for the other channels, it was calculated from previously published spectroscopic data on CH:[32–35]

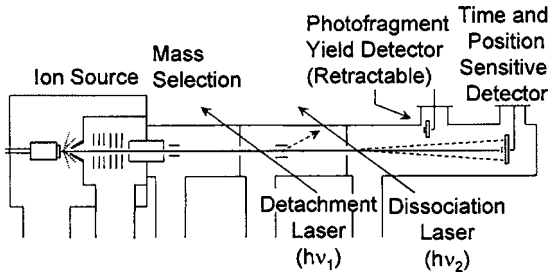

FIG. 1. Fast beam photofragment translational spectrometer.

$$\mathrm{HCNN}(\tilde{X}\,^2A'') \xrightarrow{h\nu} \mathrm{CH}(X\,^2\Pi) + \mathrm{N}_2(X\,^1\Sigma_g^+) \quad \Delta H_0 = 1.139 \pm 0.019 \text{ eV}, \tag{3}$$

$$\mathrm{CH}(a\,^4\Sigma^-) + \mathrm{N}_2(X\,^1\Sigma_g^+) \quad \Delta H_0 = 1.881 \pm 0.021 \text{ eV}, \tag{4}$$

$$\mathrm{CH}(A\,^2\Delta) + \mathrm{N}_2(X\,^1\Sigma_g^+) \quad \Delta H_0 = 4.012 \pm 0.019 \text{ eV}, \tag{5}$$

$$\mathrm{CH}(B\,^2\Sigma^-) + \mathrm{N}_2(X\,^1\Sigma_g^+) \quad \Delta H_0 = 4.370 \pm 0.019 \text{ eV}, \tag{6}$$

The formation of HCN and N is energetically allowed at all excitation energies used in this work, and formation of H and CNN is allowed at all but the lowest excitation energies.[25,36]

$$\mathrm{HCNN}(\tilde{X}\,^2A'') \xrightarrow{h\nu} \mathrm{HCN}(\tilde{X}\,^1\Sigma^+) + \mathrm{N}(^4S) \quad \Delta H_0 = 1.274 \pm 0.008 \text{ eV},$$

$$\mathrm{H} + \mathrm{CNN} \quad \Delta H_0 = 3.389 \pm 0.003 \text{ eV}.$$

However, it is difficult to observe the H+CNN channel with our coincident detection setup because of the high mass ratio, as explained in Sec. II.

Theoretical studies indicate that HCNN ($\tilde{X}\,^2A''$) and HCNN ($\tilde{A}\,^2A'$) correlate to CH($X\,^2\Pi$)+N_2($X\,^1\Sigma_g^+$) without an exit barrier.[10,16] There is, however, an exit barrier of about 1.46 eV for dissociation of HCNN ($\tilde{X}\,^2A''$) to HCN ($\tilde{X}\,^1\Sigma^+$) +N (^4S) products, a process which, in addition, requires intersystem crossing.[16]

The results of the present study reveal photofragmentation of HCNN following excitation at energies above 25 600 cm^{-1}, a range in which no previous spectroscopic studies have been performed on this radical. The only fragments seen are CH and N_2. Dissociation appears to occur following internal conversion to the ground state and/or the low lying $\tilde{A}$ state, and yields complex translational energy distributions that are not consistent with a simple model of statistical dissociation.

II. EXPERIMENT

The fast beam photofragment translational spectrometer used in these experiments (Fig. 1) has been described in detail previously.[37,38] In this instrument, we photodetach electrons from a beam of mass-selected anions to produce a

pure, internally cold beam of radicals. The radicals are then photodissociated, and the fragments are detected. This sequence can be summarized by the equation

$$HCNN^- \xrightarrow{h\nu_1} HCNN \xrightarrow{h\nu_2} \text{fragments}.$$

$HCNN^-$ ions were generated from diazomethane in a pulsed discharge source.[39] A backing gas composed of 80% Ne and 20% N_2O was passed over neat liquid diazomethane which was cooled to approximately −78 °C. Diazomethane was prepared from N-nitroso-N-methyl urea using 40 wt % NaOH (Ref. 40) and purified by distillation under vacuum. (Caution: diazomethane may undergo explosive polymerization under the conditions of this synthesis. Only clean, smooth glassware should be used and appropriate safety precautions should be exercised). Diazomethane-^{13}C was prepared from diazald-*N*-methyl-^{13}C (Aldrich) using the same procedure. The mixture of gases, at a stagnation pressure of about 2 atm, is expanded through a pulsed supersonic nozzle followed by a pulsed electrical discharge stabilized by a 1 keV electron beam.

The mixture of ions and radicals expanding from the discharge source is first collimated by a skimmer. The negative ions are then accelerated through an 8 kV potential and focused by an acceleration einzel lens. The ion of interest is selected using a Bakker-type time-of-flight mass spectrometer. Photodetachment of an electron from $HCNN^-$ is accomplished with a XeCl excimer-pumped dye laser, which, in these experiments, was tuned to 2.14 eV. From the photoelectron spectrum of $HCNN^-$,[26] we know that this detachment energy will generate HCNN in the ground electronic state, most of which will be in the ground vibrational state. After passing through the photodetachment region, the remaining ions are deflected from the beam. A second XeCl excimer-pumped dye laser is then used to photodissociate HCNN. For energies above 3.70 eV, the output of this laser is frequency-doubled. The resulting fragments are detected on one of two different detectors, depending on the type of experiment being performed.

To measure the photofragment yield (PFY) spectrum, we use a retractable 25 mm diameter chevron-stacked multichannel plate detector. The dissociation laser wavelength is scanned, and the flux of fragments impinging on the detector as a function of wavelength is recorded. The PFY spectrum of HCNN, covering the region from 25 510–40 820 cm^{-1} (245.0–392.0 nm) in 0.1 nm steps, was recorded.

Coincidence experiments on the dissociation dynamics of HCNN were performed at various photodissociation laser energies in this range using a time-and position-sensitive detector.[37,41] This detector is 40 mm in diameter with an 8 mm strip across the center which acts as a beam block, preventing the parent radicals from striking the surface. Position information is obtained by means of a wedge and strip anode assembly.[41] On this detector, the two fragments from a dissociation event are detected in coincidence, and their positions on the detector and relative times of arrival are determined. Fragment mass, translational energy, and angular distributions are determined from these data. The translational energy resolution obtainable with this apparatus under ideal conditions is $\Delta E_T/E_T=0.6\%$,[37] and the uncertainty in mass in this study, as characterized by the full width at half maximum of a single mass peak in the fragment mass distributions, is about 1.7 amu. If the ratio of the heavy fragment mass to the light fragment mass is greater than about 5:1, the fragments cannot be detected in coincidence, since either the heavy fragment will hit the beam block or the light fragment will fly clear of the detector. It should be noted that the data presented in this work were obtained before the recent upgrade to a photofragment coincidence imaging detector.[42]

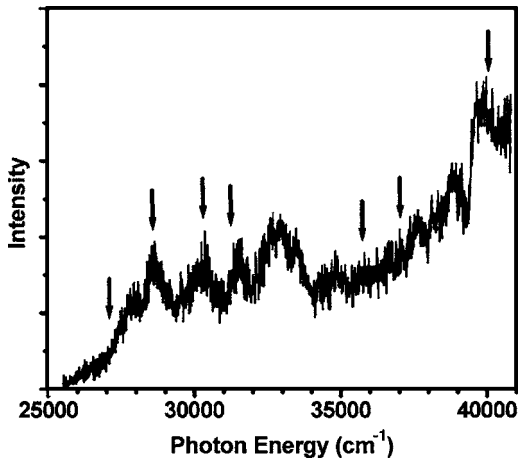

FIG. 2. Photofragment yield spectrum of HCNN. Arrows indicate the energies at which photodissociation dynamics data were taken.

III. RESULTS

A. Photofragment yield spectrum

The photofragment yield spectrum of HCNN from 25 510–40 820 cm^{-1} is shown in Fig. 2. This is the first spectrum of HCNN of any kind taken at these energies. The photofragment yield spectrum is a convolution of the absorption spectrum and the quantum yield for photodissociation as a function of wavelength. HCNN shows an onset for dissociation at about 25 600 cm^{-1}, above which dissociation is continuous, and only broad features are apparent.

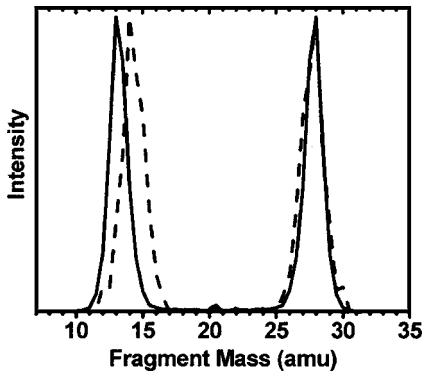

FIG. 3. Fragment mass distributions for HCNN (solid line) and $H^{13}CNN$ (dashed line).

B. Fragment mass distributions

The fragment mass distribution for HCNN obtained at an excitation energy of 3.875 eV is shown in Fig. 3. As is the case with the fragment mass distributions at all the energies studied, it shows peaks at 13 and 28 amu. This suggests that the product fragments are CH and N_2. However, our mass resolution is not good enough to distinguish the above from masses 14 and 27 amu (N and HCN fragments), or a mixture of masses 13, 14, 27, and 28 amu. Hence, in order to distinguish between these possibilities, a fragment mass distribution was obtained for $H^{13}CNN$ at an excitation energy of 3.493 eV. This is shown in Fig. 3 as a dashed line. It shows the lower mass peak shifted up by 1 amu, with the higher mass peak unchanged in mass, and both peaks unchanged in width. This confirms the assignment of the product fragments as CH and N_2.

C. Translational energy and angular distributions

The coincidence experiment yields the two dimensional fragment translational energy and angular distribution, $P(E_T,\theta)$. The translational energy distribution ($P(E_T)$) and anisotropy parameter ($\beta(E_T)$) (Ref. 43) are determined by fitting $P(E_T,\theta)$ to the equation

$$P(E_T,\theta) = P(E_T)[1+\beta(E_T)P_2(\cos\theta)], \tag{7}$$

where θ is the angle between the electric field vector of the photodissociation laser and the recoil vector between the photofragments. The anisotropy parameter $\beta(E_T)$ ranges from -1 for a $\sin^2\theta$ distribution to 2 for a $\cos^2\theta$ distribution.

Translational energy and angular distributions taken at several excitation energies are shown in Fig. 4, and these energies are marked by arrows in Fig. 2. At all excitation energies below 4.959 eV, at least two features are clearly visible in the distributions. One of these features is centered at about 1.6 eV, independent of excitation energy, and the other is broader and extends from very low energy to the highest observed translational energy. As discussed in Sec. IV A, the high-energy cutoff for all of the translational energy distributions presented in this work occurs at or very near the maximum thermodynamically allowed translational energy ($E_T^{\max}$), indicated by the dashed line I in Fig. 4. At 3.757 eV, a separate maximum close to $E_T^{\max}$ is visible above the 1.6 eV feature, and at 3.875 eV, the intensity remains quite high from the 1.6 eV feature up to a sharp cutoff just below $E_T^{\max}$. As the excitation energy is increased, the relative intensity of the broader feature grows, but the feature close to $E_T^{\max}$ rapidly diminishes.

Also shown in Fig. 4 is the anisotropy parameter β as a function of translational energy. $\beta(E_T)$ is positive for all excitation energies, and generally between about 0.3 and 1 in the translational energy range for which it can be reliably calculated. There does not appear to be a difference in $\beta(E_T)$ corresponding to the 1.6 eV feature in the translational energy distributions.

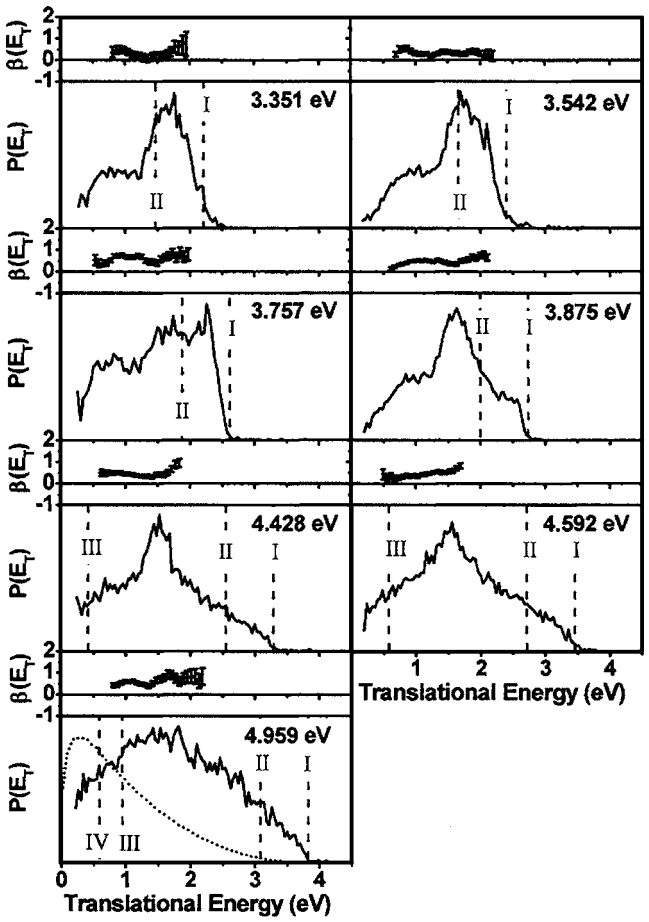

FIG. 4. Translational energy distributions ($P(E_T)$) and anisotropy parameter ($\beta(E_T)$) at the dissociation laser photon energies indicated. The dashed, vertical lines labeled I–IV indicate the maximum allowed translational energies for channels (3)–(6). The dotted line plotted with $P(E_T)$ at 4.959 eV shows the phase space theory translational energy distribution at this excitation energy.

D. Phase space theory calculations

Phase space theory[44] often gives a reasonable approximation of the product translational energy distributions that are expected if dissociation is barrierless and the available energy is statistically distributed among the available modes.[45] We have carried out phase space theory calculations for the dissociation of HCNN to $CH+N_2$ in order to determine whether a simple model describing statistical dissociation on the ground state surface is consistent with our results.

Our implementation of phase space theory has been described in detail previously.[46] The vibrational density of states is calculated using the Beyer-Swinehart algorithm, and we determine the centrifugal barrier assuming a long-range potential of the form $V(r)=-C_0/r^6$. The rotational constants and vibrational frequencies used in these calculations are given in Table I.

The phase space theory distribution for 4.959 eV is shown in Fig. 4 as a dotted line. Although the experimental $P(E_T)$ at this energy shows only the broader feature, it is not at all well fit by the phase space theory distribution and peaks at higher energy. Phase space theory distributions were also calculated for lower excitation energies, and in all cases

TABLE I. Constants (in cm^{-1}) used in phase space theory calculations.

	Vibrational frequency	Rotational constant(s)
HCNN[a]		20.504, 0.412, 0.403
CH[b]	2858.5	14.457
N_2[b]	2358.57	1.99824

[a]Reference 26.
[b]Reference 53.

the broad feature in the experimental translational energy distribution peaked at higher energy than the phase space theory distribution.

IV. DISCUSSION

A. Heat of formation of HCNN

The translational energy distributions in Fig. 4 show cutoffs at high translational energy which increase additively with increasing excitation energy. This allows us to use the maximum translational energy to determine the bond dissociation energy and the heat of formation of HCNN. For channel (3) products (CH and N_2 in their ground electronic states), conservation of energy dictates that the maximum allowed translational energy, at an excitation energy $h\nu$ is given by

$$E_T^{\max} = h\nu - D_0,$$

where D_0 is the dissociation energy for the bond cleaved in the photodissociation event, that is, HC–NN in all the distributions taken in this study.

Since the translational energy distributions taken at 3.647 (not shown), 3.757, and 3.875 eV have the sharpest cutoffs at high translational energy, these have been used, along with the assumption that the cutoffs correspond to products with no rotational or vibrational excitation, to determine D_0. The value of D_0 obtained in this way is 1.139 ± 0.019 eV. Together with the heat of formation of CH, 6.149 ± 0.013 eV,[36,47] this yields a heat of formation, $\Delta_f H_0(\mathrm{HCNN}) = 5.010 \pm 0.023$ eV, in agreement with the value of 5.02 ± 0.18 eV previously reported,[25] but with much less uncertainty. The values of $E_T^{\max}$ for channel (3) products ($\mathrm{CH}(X\,^2\Pi) + \mathrm{N_2}(X\,^1\Sigma_g^+)$) calculated from this value of D_0 are shown as dashed, vertical lines in Fig. 4, and agree well with the high translational energy cutoffs. This agreement, observed here over a wide range of excitation energies, reinforces the assumption that the fastest products have no internal energy.

B. Nature of the electronic transition

Since little is known about the electronically excited states of HCNN, we will discuss the electronic transition excited in these experiments on the basis of information on the isoelectronic species HCCO. The molecular orbital configurations of the four lowest lying electronic states of HCCO have been described previously.[48] The ground state of HCCO has C_s symmetry with the electronic configuration $\ldots(6a')^2(7a')^2(8a')^2(1a'')^2(9a')^2(2a'')^1$. As is the case with HCNN, the two lowest electronic states are a Renner-Teller pair, although in the case of HCCO the $\tilde{A}\,^2A'[^2\Pi]$ state, with the electronic configuration $\ldots(6\sigma)^2(7\sigma)^2(1\pi_x)^2(1\pi_y)^2(2\pi_x)^1(2\pi_y)^2$, has a linear equilibrium geometry. The $9a'$ and $2a''$ (CCO π) orbitals become degenerate at linearity, as do the $8a'$ and $1a''$ (CO π) orbitals. The $\tilde{B}\,^2\Pi$ state results from the promotion of an electron from a CO π orbital to a CCO π orbital, resulting in the electronic configuration $\ldots(6\sigma)^2(7\sigma)^2(1\pi)^3(2\pi)^4$.

Szalay *et al.*[49] have shown on the basis of *ab initio* calculations that the $\tilde{B}\,^2\Pi$ state of HCCO does not undergo Renner-Teller distortion and may be treated as a single electronic state. Osborn *et al.*[48] carried out photodissociation experiments on HCCO, and assigned the transition excited in the those experiments to the $\tilde{B}\,^2\Pi \leftarrow \tilde{X}\,^2A''$ band. Because of the similarities in the photodissociation spectroscopy and dynamics of these two radicals (see Sec. IV D), it is likely that the transition excited in our experiments on HCNN is similar to the HCCO $\tilde{B}\,^2\Pi \leftarrow \tilde{X}\,^2A''$ transition, and involves a transition from a bonding orbital to a nonbonding orbital in the CNN π system. It is not possible to determine the symmetry of the upper state on the basis of our data. However, since the anisotropy parameters determined at different excitation energies are similar, it is unlikely that the symmetry of the transition dominating the photofragment yield changes with increasing excitation energy (as would happen, for example, if the upper state as a Renner-Teller pair consisting of A'' and A' components, close enough in energy that we accessed both states, and both had comparable photofragment yields). Since there is no spectroscopic information available for the 1.85–3.16 eV region for HCNN, and there are no theoretical predictions for the energy of the $\tilde{B}$ state, assignment of the transition observed in the photofragment yield spectrum as $\tilde{B}\,^2A''(A') \leftarrow \tilde{X}\,^2A''$ or $\tilde{B}\,^2\Pi \leftarrow \tilde{X}\,^2A''$ is tentative. The onset of dissociation, at roughly 3.17 eV, provides an upper limit for the origin of this electronic band, since it is possible that the quantum yield for photodissociation close to the origin is too low for any fragments to be detected.

C. Dissociation mechanism

The formation of CH and N_2 in the photodissociation of HCNN is not surprising, since these are the most thermodynamically favored products and their formation involves no rearrangement. However, based on the translational energy distributions, the dissociation dynamics appear to be complex. The dynamics will be discussed in more detail in this section in an attempt to elucidate the dissociation mechanism.

The maximum allowed translational energies for various channels can help in determining the electronic states of the product fragments leading to a given feature in the translational energy distributions. In Fig. 4, the maximum allowed translational energies for channels (3)–(6), calculated from the heats of reaction given in Sec. I, are shown as vertical dashed lines labeled I–IV. From the distribution measured at an excitation energy of 3.351 eV, it is apparent that the feature centered at about 1.6 eV is due to CH and N_2 formed in their ground electronic states [channel(3)]. In the distribu-

tions taken at 3.875 eV and above, it is clear that the broader feature has some intensity above the cutoff for CH ($a\,^4\Sigma^-$) $+N_2$ [channel (4)], and therefore also appears to be due to CH and N_2 fragments in their ground electronic states.

From these observations, we can begin to piece together the most likely dissociation mechanism. The only states of HCNN correlating to CH and N_2 in their ground electronic states are the $\tilde{X}\,^2A''$ and $\tilde{A}\,^2A'$ states. Therefore, if only fragments in their ground electronic states are formed, it appears that internal conversion is taking place from the initial excited state to one or both of these states before dissociation. The anisotropic photofragment angular distributions seen here suggest that dissociation from the ground state is rapid on a time scale of molecular rotation, i.e., a time scale on the order of a few picoseconds. In addition, analysis of the $P(E_T)$ distributions can provide insight into whether dissociation is more rapid than the faster time scale required for vibrational energy randomization on the ground state, the condition required for statistical models of dissociation to apply.[45] This assumption can be tested by comparing the experimental $P(E_T)$ distributions to those obtained from phase space theory, a reasonable statistical model to apply since there is no exit barrier to dissociation of either HCNN($\tilde{X}\,^2A''$) or HCNN($\tilde{A}\,^2A'$) to ground state CH and N_2. In fact, as shown in Fig. 4, the experimental distributions do not agree with a phase space theory calculation. It has been observed[50] that phase space theory may underestimate the average fragment translational energy when the excitation energy is well above the bond dissociation energy, at least in part as a result of the tightening of the critical geometry[51] as the excess energy increases. However, the multiple features present in the $P(E_T)$ distributions at energies below 4.959 eV seem unlikely to conform to any statistical model. The explanation for the fact that dissociation is rapid—and appears nonstatistical—may lie in the fact that the excitation energy is well in excess of (roughly 2–4 eV above) the bond dissociation energy.

While we can rationalize the nonstatistical appearance of the translational energy distributions, it is less apparent what the form of the $P(E_T)$ distributions—the presence of a feature near 1.6 eV in addition to the broad feature, and the fact that the broad feature grows in relative intensity with increasing excitation energy—implies for the dissociation mechanism. The presence of two components in many of the $P(E_T)$ distributions may reflect dissociation on both the $\tilde{X}\,^2A''$ and $\tilde{A}\,^2A'$ electronic states. Neither state has an exit barrier with respect to $CH+N_2$ products, but the dissociation dynamics on the $\tilde{A}\,^2A'$ state should be more direct since it is less strongly bound than the $\tilde{X}\,^2A''$ state. Moreover, as pointed out in the Introduction, the equilibrium geometries of the two states are quite different, which could also lead to different translational energy distributions. In any case, the attribution of the two components to the two electronic states is appealing but must be regarded as tentative. It is also possible, for example, that the two components result from two ensembles of molecules generated on the ground state by different internal conversion pathways.

D. Comparison with HCCO

It is informative to compare the photodissociation dynamics and spectroscopy of HCNN with those of the isoelectronic radical HCCO, which was the subject of a previous study by this group.[48] HCNN and HCCO have similar ground state geometries and both have a low-lying $\tilde{A}\,^2A'$ state which forms a Renner-Teller pair with the ground state.

Comparison of the photofragment yield spectra of HCNN and HCCO shows some similarities. In both cases, the photofragment yield generally increases with excitation energy above the onset, and shows broad, unresolved features with spacings of roughly 1000–2000 cm^{-1}. In the case of HCCO, vibrational structure was visible in the photofragment yield spectrum in the lowest 4000 cm^{-1} above the onset, and rotational structure was resolved in some of the vibrational transitions. No such structure appears in the photofragment yield spectrum of HCNN. HCCO shows an onset at somewhat higher excitation energy (33 424 versus 25 600 cm^{-1} for HCNN).

The fragments from the photodissociation of HCCO were identified as CH+CO, with features attributed to $CH(X\,^2\Pi)+CO(X\,^1\Sigma^+)$ dominating at all but the lowest excitation energies. These products are analogous to the $CH(X\,^2\Pi)+N_2(X\,^1\Sigma_g^+)$ products seen in this study for HCNN dissociation, although the HC–CO bond dissociation energy is much higher than that for HC–NN (3.14 versus 1.139 eV). The fragment translational energy distributions at various energies also show striking similarities. In the case of HCCO, a bimodal distribution is seen at low excitation energies, and the broader, lower translational energy feature dominates as the excitation energy is increased. Except for the absence of a feature near $E_T^{\max}$, this pattern is qualitatively the same as the trend seen in the translational energy distributions for HCNN. In addition, the anisotropy parameters are above zero at all excitation energies for both radicals. At the lowest excitation energies studied, near the onset for dissociation, HCCO photodissociation showed a contribution from a different channel, $CH(a\,^4\Sigma^-)+CO(X\,^1\Sigma^+)$, implying that intersystem crossing takes place in HCCO at these low excitation energies. No evidence for intersystem crossing is seen in the photodissociation dynamics of HCNN.

As is the case with HCNN, a definitive conclusion on the reasons for the bimodal distributions in the photofragment translational energy distributions for HCCO was not reached. It could be the result of internal conversion to a single state, $\tilde{X}\,^2A''$, for example, with two distinct ensembles, or a combination of internal conversion to the $\tilde{X}\,^2A''$ and $\tilde{A}\,^2A'$ states. In HCCO, in contrast to HCNN, the $\tilde{X}\,^2A''$ and $\tilde{A}\,^2A'$ states are very close in energy, and are relatively strongly bound, by 3.14 and 3.06 eV,[49,52] respectively, relative to CH+CO products. On the other hand, the geometries of HCNN and HCCO are similar in both the $\tilde{X}\,^2A''$ and the $\tilde{A}\,^2A'$ states (for HCCO, the $\tilde{A}\,^2A'$ state is linear,[49] and for HCNN, the $\tilde{A}\,^2A'$ is nearly linear[16]). Thus, if the two components of the $P(E_T)$ distributions arise from dissociation on the $\tilde{X}\,^2A''$ and $\tilde{A}\,^2A'$

states for both species, it seems likely that geometric effects are more important than energetic effects in determining the form of these distributions.

E. Comparison with HNCN

The photodissociation dynamics of another HCN_2 isomer, HNCN, were previously studied in this laboratory.[24] As is the case for HCNN, CH ($X\,^2\Pi$) and N_2 ($X\,^1\Sigma_g^+$) products were observed. Although the products were the same in these two cases, the dynamics were quite different. The $P(E_T)$ distributions found for HNCN showed vibrational resolution of the N_2 stretch, indicating that there was little rotational excitation. This implies that dissociation took place from a transition state in which torque was not applied to the N_2 fragment. According to calculations by Cui and Morokuma,[16] the transition state between *c*-HCNN and $CH+N_2$ fits this criterion. As expected in a process involving extensive rearrangement, the angular distributions found for HNCN dissociation were isotropic at all excitation energies studied. This is in contrast to the angular distributions for HCNN, which showed consistently positive anisotropy parameters. It appears from these results that while HCNN and HNCN fall apart to the same products, they sample very different regions of the $CH+N_2$ potential energy surface in the process. The difference in the dissociation dynamics of these two radicals is consistent with the results of Cui and Morokuma[16] and Moskaleva *et al.*[13] which show completely different pathways on the ground state for dissociation of these two radicals to $CH+N_2$, and supports the conclusion that HNCN does not rearrange to HCNN prior to dissociation.

V. CONCLUSIONS

We have investigated the photodissociation dynamics of the HCNN free radical. Dissociation takes place following a transition which is tentatively assigned as $\tilde{B}\leftarrow\tilde{X}\,^2A''$. Photofragments are observed for excitation energies above 25 600 cm^{-1}, indicating that the origin of the absorption band lies at or below this energy. All excitation energies studied lead to the formation of $CH(X\,^2\Pi)+N_2(X\,^1\Sigma_g^+)$ as the only detectable products. The fragment translational energy distributions are not well fit by phase space theory, and show at least two distinct features at lower excitation energies. The angular distributions show that dissociation is rapid on a rotational time scale.

Since the products are formed in their ground electronic states, and only the $\tilde{X}\,^2A''$ and $\tilde{A}\,^2A'$ states correlate to these product states, the dissociation mechanism appears to involve internal conversion to one or both of these states. The complex appearance of the translational energy distributions indicates that dissociation then proceeds rapidly, before redistribution of the excess energy among the available modes is complete. We propose that the two components to the translational energy distributions observed over a wide range of excitation energies arise either from dissociation on the $\tilde{X}\,^2A''$ and $\tilde{A}\,^2A'$ states, or by two ensembles of molecules created on the ground state by different internal conversion pathways.

ACKNOWLEDGMENT

This work was supported by the Director, Office of Basic Energy Sciences, Chemical Sciences Division of the U.S. Department of Energy under Contract No. DE AC02-05CH11231.

[1] J. A. Miller and C. T. Bowman, Prog. Energy Combust. Sci. **15**, 287 (1989).
[2] C. P. Fenimore, *13th Symposium (International) on Combustion* (The Combustion Institute, Pittsburgh, 1971), p. 373.
[3] M. R. Berman and M. C. Lin, J. Phys. Chem. **87**, 3933 (1983).
[4] A. J. Dean, R. K. Hanson, and C. T. Bowman, *23rd Symposium (International) on Combustion* (The Combustion Institute, Pittsburgh, 1990), p. 259.
[5] D. Lindackers, M. Burmeister, and P. Roth, *23rd Symposium (International) on Combustion* (The Combustion Institute, Pittsburgh, 1990), p. 251.
[6] L. J. Medhurst, N. L. Garland, and H. H. Nelson, J. Phys. Chem. **97**, 12275 (1993).
[7] D. Fulle and H. Hippler, J. Chem. Phys. **105**, 5423 (1996).
[8] S. D. Le Picard, A. Canosa, B. R. Rowe, R. A. Brownsword, and I. W. M. Smith, J. Chem. Soc., Faraday Trans. **94**, 2889 (1998).
[9] J. A. Miller and S. P. Walch, Int. J. Chem. Kinet. **29**, 253 (1997).
[10] J. M. L. Martin and P. R. Taylor, Chem. Phys. Lett. **209**, 143 (1993).
[11] M. R. Manaa and D. R. Yarkony, J. Chem. Phys. **95**, 1808 (1991).
[12] M. R. Manaa and D. R. Yarkony, Chem. Phys. Lett. **188**, 352 (1992).
[13] L. V. Moskaleva, W. S. Xia, and M. C. Lin, Chem. Phys. Lett. **331**, 269 (2000).
[14] L. V. Moskaleva and M. C. Lin, Z. Phys. Chem. **215**, 1043 (2001).
[15] L. V. Moskaleva and M. C. Lin, Proc. Combust. Inst. **28**, 2393 (2000).
[16] Q. Cui and K. Morokuma, Theor. Chem. Acc. **102**, 127 (1999).
[17] Q. Cui, K. Morokuma, J. M. Bowman, and S. J. Klippenstein, J. Chem. Phys. **110**, 9469 (1999).
[18] T. Seideman and S. P. Walch, J. Chem. Phys. **101**, 3656 (1994).
[19] T. Seideman, J. Chem. Phys. **101**, 3662 (1994).
[20] A. S. Rodgers and G. P. Smith, Chem. Phys. Lett. **253**, 313 (1996).
[21] A. Wada and T. Takayanagi, J. Chem. Phys. **116**, 7065 (2002).
[22] J. Blauwens, B. Smets, and J. Peeters, *16th Symposium (International) on Combustion* (The Combustion Institute, Pittsburgh, 1977), p. 1055.
[23] T. Takayanagi, Chem. Phys. Lett. **368**, 393 (2003).
[24] R. T. Bise, A. A. Hoops, and D. M. Neumark, J. Chem. Phys. **114**, 9000 (2001).
[25] R. T. Bise, A. A. Hoops, H. Choi, and D. M. Neumark, J. Chem. Phys. **113**, 4179 (2000).
[26] E. P. Clifford, P. G. Wenthold, W. C. Lineberger, G. A. Petersson, K. M. Broadus, S. R. Kass, S. Kato, C. H. DePuy, V. M. Bierbaum, and G. B. Ellison, J. Phys. Chem. A **102**, 7100 (1998).
[27] J. F. Ogilvie, Can. J. Chem. **46**, 2472 (1968).
[28] J. F. Ogilvie, Photochem. Photobiol. **9**, 65 (1969).
[29] L. B. Herbert, I. R. Sims, I. W. M. Smith, D. W. A. Stewart, A. C. Symonds, A. Canosa, and B. R. Rowe, J. Phys. Chem. **100**, 14928 (1996).
[30] P. E. Fleming, Chem. Phys. Lett. **321**, 129 (2000).
[31] C. Puzzarini and A. Gambi, J. Chem. Phys. **122**, 064316 (2005).
[32] G. Herzberg and J. W. C. Johns, Astrophys. J. **158**, 399 (1969).
[33] A. Kasdan, E. Herbst, and W. C. Lineberger, Chem. Phys. Lett. **31**, 78 (1975).
[34] R. Kepa, A. Para, M. Rytel, and M. Zachwieja, J. Mol. Spectrosc. **178**, 189 (1996).
[35] M. Zachwieja, J. Mol. Spectrosc. **170**, 285 (1995).
[36] M. W. Chase, Jr., J. R. Downey, Jr., D. J. Fruip, R. A. McDonald, and A. N. Syverud, *JANAF Thermochemical Tables*, 3rd ed. (AIP, New York, 1985); [J. Phys. Chem. Ref. Data **14**, Suppl. 1, (1985)].
[37] D. J. Leahy, D. L. Osborn, D. R. Cyr, and D. M. Neumark, J. Chem. Phys. **103**, 2495 (1995).
[38] R. E. Continetti, D. R. Cyr, R. B. Metz, and D. M. Neumark, Chem. Phys. Lett. **182**, 406 (1991).
[39] D. L. Osborn, D. J. Leahy, D. R. Cyr, and D. M. Neumark, J. Chem. Phys. **104**, 5026 (1996).
[40] W. H. Urry and J. R. Eizner, J. Am. Chem. Soc. **74**, 5822 (1952).
[41] R. E. Continetti, D. R. Cyr, D. L. Osborn, D. J. Leahy, and D. M. Neumark, J. Chem. Phys. **99**, 2616 (1993).

[42] A. A. Hoops, J. R. Gascooke, A. E. Faulhaber, K. E. Kautzman, and D. M. Neumark, Chem. Phys. Lett. **374**, 235 (2003).
[43] R. N. Zare, Mol. Photochem. **4**, 1 (1972).
[44] P. Pechukas and J. C. Light, J. Chem. Phys. **42**, 3281 (1965).
[45] T. Baer and W. L. Hase, *Unimolecular Reaction Dynamics* (Oxford University Press, Oxford, 1996).
[46] H. Choi, R. T. Bise, A. A. Hoops, D. H. Mordaunt, and D. M. Neumark, J. Phys. Chem. A **104**, 2025 (2000).
[47] M. Danielsson, P. Erman, A. Hishikawa, M. Larsson, R.-K. E. Sumame, and G. Sundström, J. Chem. Phys. **98**, 9405 (1993).
[48] D. L. Osborn, D. H. Mordaunt, H. Choi, R. T. Bise, D. M. Neumark, and C. M. Rohlfing, J. Chem. Phys. **106**, 10087 (1997).
[49] P. G. Szalay, G. Fogarasi, and L. Nemes, Chem. Phys. Lett. **263**, 91 (1996).
[50] L. Bonnet, P. Larrengaray, and J.-C. Rayez, Phys. Chem. Chem. Phys. **7**, 3540 (2005).
[51] W. L. Hase, J. Chem. Phys. **64**, 2442 (1976).
[52] D. H. Mordaunt, D. L. Osborn, H. Choi, R. T. Bise, and D. M. Neumark, J. Chem. Phys. **105**, 6078 (1996).
[53] K. P. Huber and G. Herzberg, *Constants of Diatomic Molecules* (Van Nostrand Reinhold, New York, 1979).